

Research Paper

# Mathematical Modelling of MHD Blood Flow with Gold Nanoparticles in Slip Small Arteries

Wan Faezah Wan Azmi<sup>✉</sup>, Ahmad Qushairi Mohamad<sup>✉</sup>, Lim Yeou Jiann<sup>✉</sup>, Sharidan Shafie<sup>✉</sup>

Department of Mathematical Sciences, Faculty of Science, Universiti Teknologi Malaysia, 81310 UTM Johor Bahru, Johor, Malaysia  
Email: wanfaezah@graduate.utm.my (W.F.W.A.); ahmadqushairi@utm.my (A.Q.M.); jiann@utm.my (L.Y.J.); sharidan@utm.my (S.S.)

Received July 02 2023; Revised September 28 2023; Accepted for publication October 04 2023.

Corresponding author: A.Q. Mohamad (ahmadqushairi@utm.my)

© 2023 Published by Shahid Chamran University of Ahvaz

**Abstract.** Nanofluid is an innovative technology that is essential in biomedical applications. A nanofluid study of human blood flow mathematically is more favorable since it provides a hypothesis for complex systems faster and is cost-saving. Academic researchers have expressed interest in investigating the characteristics of Casson nanofluid flow within a cylindrical structure, which serves as a representative model for the flow of blood in constricted human arteries. However, slip velocity boundary conditions were considered by only a certain number of researchers. The goal of this study is to develop mathematical modelling of Casson fluid flow with gold nanoparticles in the slip cylinder. The impacts of convective heat transfer, magnetohydrodynamics (MHD), and porous medium are also investigated. The Tiwari-Das nanofluid model is utilized in the governing equations. Then, the governing equations with the related boundary conditions are transformed into dimensionless form. The analytical solutions were obtained through the use of the Laplace transform and the finite Hankel transform in combination. The results of nanofluid velocity, temperature, skin friction, and Nusselt number are analyzed through the use of graphs and tables containing relevant parameters. Slip velocity causes an increment in blood velocity and a decrement in skin friction. Blood velocity and temperature are enhanced as the nanoparticles' volume fraction is increased. It is significant in cancer treatment to increase the heat transfer rate at targeted cancerous cells.

**Keywords:** Casson nanofluid, slip cylinder, Laplace transform, finite Hankel transform, MHD blood flow.

## 1. Introduction

The human body is a complicated system that contains biofluid, which accounts for 58% to 80% of total body weight. Biofluid is a complex fluid flow within living tissue such as blood, saliva, human milk, urine, and amniotic fluid [1, 2]. Since biofluid is a complex fluid, it falls under the non-Newtonian fluid category. This phenomenon contradicts Newton's law of viscosity and exhibits an inverse relationship with both shear stress and shear rate [3]. Due to their highly significant biomedical applications, non-Newtonian fluid problems have attracted a lot of attention over the past few years. However, there is no constitutive equation that governs all the characteristics of the blood. This has led to the development of numerous constitutive equations for blood [4]. The selection of a fluid model is a simplification of the intricate behaviour of blood, which can demonstrate diverse characteristics in different conditions. Blood exhibits distinct properties, demonstrating solid-like behaviour at low shear rates or when it is stationary, and fluid-like behaviour at higher shear rates during flow. At exceedingly low shear rates, blood tends to exhibit nearly adhesive properties, owing to inter-component forces and impeding its flow. This phenomenon is commonly referred to as the yield stress [5, 6]. The Casson fluid model is commonly used in blood flow modelling due to its accurate representation of the blood yield stress and its ability to capture the transition between solid-like and fluid-like properties. The Casson fluid demonstrates characteristic behaviour that can be classified as both shear-thinning and yield stress, indicating the minimum shear stress needed to initiate flow. The fluid exhibits solid-like behaviour below the yield stress and fluid-like behaviour above it. Casson fluid model are frequently used to mimic blood flow in narrowed blood vessels. It accurately describes blood flow characteristics in the capillaries with a diameter of 130–1000  $\mu\text{m}$  [7, 8]. Therefore, it is commonly used in research to mathematically simulate the behaviour of blood flow in situations where it is slow or stagnant, such as in small arteries [9, 10].

For the past decades, mathematical modelling has been used by researchers to explore the heat transport phenomena within the human body. The process by which the body tries to maintain its internal temperature at an average of 37 degrees Celsius is known as thermoregulation. It refers to the body's ability to gain and lose heat [11]. Heat transfer processes in the human body involve thermal conduction, convection, radiation, evaporation, and metabolism [12]. Luchakov and Nozdrachev [13] used a mathematical model to investigate heat transportation in the human body. They highlighted that conductive heat transfer is common in surface tissue, while convective heat transfer is common in core tissues, which consist of 85% blood. Since the current study involves blood circulation, free convection is considered. The purpose of free convection is to naturally equalise the



temperature between hot and cold regions. Researchers are interested in theoretically exploring the issue of free convection blood flow using the Casson fluid model in cartesian coordinates. They presented a numerical mathematical model for this purpose [14, 15].

One of the heat exchange mechanisms in the human body is magnetohydrodynamics (MHD). The MHD study pertains to the investigation of physical phenomena exhibited by fluids that conduct electricity, for example salt water, plasmas, and liquid metals [16]. In human blood, plasma accounts up 55% of the total volume, whereas red blood cells (RBCs), white blood cells (WBCs), and platelets each make up 45% of the total volume. Plasma, also known as conductive viscous fluid, consists of various substances such as salt, proteins, hormones, and others [17]. Hence, Abdalla et al. [18] stated that the concept of blood refers to the insulated cells floating in the conducting fluid. When an electrically conducting fluid flows over a natural or man-made magnetic field, an induced current is generated. The human body generates a natural magnetic field through the activity of the heart and brain, while man-made magnetic fields are produced by electromagnetic devices like a television, laptop, or mobile phone [19, 20]. The presence of an induced current within a magnetic field gives rise to a resistive force, commonly referred to as the Lorentz force. It was proposed by Hartmann in 1937 [21]. The advantages of MHD in regulating blood flow behaviour and heat transfer characteristics in the human body were exploited by several researchers. Its significance is essential in the realm of medical science implementations such as cancer tumour treatment, drug delivery, regulating blood flow during surgery, laser beam scanning, and others [22]. Ali et al. [23–25] explored analytically the magnetic field impact on the blood flow in small blood vessels by considering convective heat transfer. They modelled the blood using the Casson fluid model. The researchers examined multiple boundary circumstances, including those involving fixed, moving, and oscillating cylinders. They found that blood flow decreased by increasing the magnetic field. Then, Kumar and Rizvi [26] investigated a numerically similar problem as Ali et al. [24] by considering moving cylinders and gained the same result.

The incorporation of a porous medium has been noted to augment the convective heat transfer phenomena in various scenarios that entail the transportation of biofluids. A porous medium refers to a substance that comprises a solid matrix featuring interconnected voids such as blood clots, cholesterol plaques, and excess fat. In other words, permeable media have pores that alter the biofluid flow. The use of permeability in biological fluids, tissues, and organs are important in contemporary research, such as the chromatographic process (protein separation to purify the blood components) [27–29]. Hence, it attracted many researchers to further study these issues in blood flow stimulation. Dash et al. [30] are among the earliest researchers to study the Casson fluid flow in a porous medium of fixed cylinder. They solved the problems numerically and stated that the obtained results are significant in the Pathological scenarios involving blood flow within the coronary artery, featuring the occurrence of fatty or cholesterol plaques. Later, Anurag et al. [31, 32] extended a similar problem as Dash et al. [30] by considering free convection flow in the problem. The problem was resolved through analytical means, leading to the conclusion that the rise in Darcy number causes increase in the fluid velocity, attributable to the rise in media permeability. Raje et al. [33] explored Casson fluid flow in the porous cylinder with the effect of MHD and generation of internal heat and entropy. They obtained that temperature profile incline with the increment of Casson parameter.

Recently, there has been a notable surge of interest among researchers in enhancing heat transmission mechanisms in a variety of fields by introducing one of the innovative technologies known as nanofluid technology. The attention directed towards nanofluids is driven by their capacity to enhance heat transfer rates in engineering systems, while also effectively addressing concerns such as erosion, sedimentation, and blockage that were prominent issues in prior solid-liquid mixtures containing larger particulates [34–36]. Nanofluid is a new kind of fluid that comprises two components which are base fluid and solid nanoparticles, which were first described by Choi and Eastman in 1995 [37]. The proposed approach focuses on improving the thermal conductivity properties of the base fluid by incorporating solid nanoparticles with a high degree of thermal conductivity [38–40]. Nanomedicine is a new discipline that has emerged as a result of nanotechnologies. It primarily focuses on improving or changing illness detection, diagnosis, treatment, and prevention at the cellular level of the human body [41]. Examples of its applications are drug delivery, cancer therapeutics, nano-cryosurgery, sensing, and imaging [42]. Researchers are attentive to studying further nanofluid problems in various geometries due to their high significance in medical science applications. Hence, Casson nanofluid flow in cylindrical form is the closest related to the blood flow application. Malik et al. [43] are among the earliest researchers to numerically study Casson nanofluid flow in the stretching cylinder with a heat transmission. Then, Alebraheem and Ramzan [44] explored the numerically swirling flow of Casson nanofluid past a cylinder with the MHD effect. A similar problem has been extended by Khan et al. [45] with the stretchable and rotation cylinders. Walegign [46] solved analytically Casson nanofluid flow over an inclined stretched cylinder with the effects of MHD, chemical reaction, and heat transfer. Farooq et al. [47] compared numerically the effect of Casson nanofluid flow on the stretching cylinder and plate. They considered the effects of MHD, bioconvection, exponential heat sink/source and microorganisms. Alharbi et al. [48] solved numerically the problem of Casson nanofluid flow between two cylinders with the similar effect as [47] which is additional of microorganisms. All of them employed Buongiorno's nanofluid model in their momentum governing equation.

Moreover, Mahdi et al. [49] and Kasaeian et al. [50] highlighted that nanofluid flow in the porous medium has significant potential to improve heat transmission. The heightened rate of heat transfer is ascribed to the expanded contact surface area between the porous structure and the flow of nanofluid. Besides that, some other factors influence heat transfer rates, such as nanoparticle (NPs) size, NPs shape, NPs volume fraction, and NPs type [51]. Recent research has shown that liquids with metallic or nonmetallic solid nanoparticles have increased heat conductivity relative to the base liquid [52]. Metallic nanoparticles, exemplified by gold and silver, are expected to enhance tissue conductivity in a moist biological environment. The proper selection of the NPs type is essential to avoid any toxicological effect due to free radical production from NPs [53]. Gold (Au) NPs become the preferred NPs type when it comes to the blood flow issue. It is because Au NPs have high biocompatibility, biodegradability, stability, and thermal conductivity [54, 55]. Au NPs are significant for improved medical diagnostic imaging, improved drug delivery treatment, and boosting tumour-killing efficiency either by using cryosurgery or hyperthermia [56–58]. Researchers explored the blood flow behaviour with the dispersion of the Au NPs in different types of geometries. For example, Khan et al. [59, 60] studied numerically the behaviour of the blood flow with the dispersion of the Au NPs over a rotating stretchable disc. They modelled blood flow using the Casson fluid model. They also considered MHD and porosity effects. They found that nanoparticles and Casson parameters enhanced blood velocity. The numerical impact of Au NPs on blood flow, modelled as a Casson fluid, was investigated by Hussain et al. [61] in their study. They analysed the blood flow at the stagnation point and included the EMHD (electromagnetohydrodynamics) effect. Besides, Hussain et al. [62] explored the dynamics of Casson blood flow while incorporating a suspension of Au NPs passed through between two inclined plates (channel) with the MHD effect. They obtained an exact solution and stated that blood velocity is supported by Au NPs. Upreti et al. [63] explored numerically the stagnation point flow of Casson blood fluid with dispersion of Au NPs flow on the stretching sheet. They considered the MHD and porous medium effects, and Cattaneo-Christov model. Imtiaz et al. [64] performed an analytical study on Casson blood flow with the presence of Au NPs in a cylindrical context.



All of the studies above assumed that no slip occurred at the boundary. The assumption of fluid flow without slip means they stick to the boundary and have a continuous velocity profile throughout the adjacent region, according to the general hypothesis in fluid mechanics [65]. Nubar [66] highlighted that this hypothesis applies to the Newtonian fluid only. Some researchers discovered that the fluid-solid interface has a finite velocity, and a particular kind of velocity boundary condition is known as a slip boundary. The phenomenon under consideration pertains to the dynamic interaction within the close proximity of a solid surface and the surrounding fluid, which constitutes a critical interfacial property that can significantly influence the flow characteristics of the fluid [67]. Navier was the first person to introduce slip boundary conditions in his early study in 1823 on linear viscous fluid [68]. The occurrence of fluid flow with a slip boundary has garnered significant interest in the context of biomedical technological issues, particularly in relation to the refinement of artificial mechanical heart valve surfaces and internal cavities [68]. Besides, modelling blood flow in the arteries also needs to consider the existence of a slip boundary since it is close to real-life problems. As a result, many researchers paid special attention to including slip conditions for different geometries of their problems. For example, Afify [69] investigated the numerical slip boundary effect on the Casson nanofluid flow over a stretching sheet. Gbadeyan *et al.* [70] explored numerically the impact of the slip boundary on the Casson nanofluid flow passing through the vertical plate. They considered the effects of MHD, porosity, radiation, and chemical reactions. They found that slip velocity would enhance velocity profiles. Later, the slip velocity effect occurred in the channel for Casson nanofluid, which was examined numerically by Noor *et al.* [71]. They considered MHD and porous medium effects. Thirupathi *et al.* [72] studied Casson nanofluid flow on the slip stagnation point with the effects of MHD, radiation, and chemical reactions. Besides, Usman *et al.* [73] discovered that Casson nanofluid velocity increases with slip velocity. It flows on the inclined stretching cylinder with the MHD effect, heat, and mass transfer. Iqbal *et al.* [74] studied a numerically similar problem as [73] with different effects of suction and blowing on the boundary layer. All of the studies above employed Buongiorno's nanofluid model. Besides, Azmi *et al.* [75] investigated analytically blood Casson nanofluid flow in a slip cylinder by employing the Tiwari and Das model. They obtained that Casson nanofluid velocity increases by increasing the slip velocity parameter.

Researchers investigate nanofluid technology either experimentally or mathematically to regulate the heat transmission process. Investigating through mathematical modelling plays a vital role in formulating real-life situations, solving complex problems, and providing an early hypothesis for the experiments. According to a thorough review of the literature, the effect of slip velocity on the Casson fluid with gold nanoparticles flowing in the porous medium of the cylinder has not been studied previously. Since Au NPs are considered in this study, it is the best way to develop mathematical modelling for this problem due to time and cost consumption. Hence, the objective of this investigation is to construct a mathematical model and conduct an analytical analysis of the issue of unsteady blood flow containing Au NPs within a slip cylinder. The utilization of the Casson fluid model is prevalent in the computational modelling of hemodynamics in narrowed blood arteries. The effects of the heat transfer process, pulsatile pressure gradient, MHD, and porosity are involved in this study. The significance of this study lies in its theoretical exploration of issues associated with blood diseases, such as blood clots and tumors. This investigation plays a pivotal role in simulating early predictions and formulating hypotheses before embarking on practical treatments like nano-cryosurgery and hyperthermia. Consequently, medical practitioners can anticipate potential outcomes that may arise during the actual treatment procedures. The present study utilises the Tiwari-Das nanofluid model. To accomplish the aim of the investigation, the governing equations pertaining to the problem are initially transformed into dimensionless form through the use of suitable dimensionless variables. Later, analytical solutions of the blood flow are obtained by combining Laplace transform and finite Hankel transform techniques. Then, the numerical solutions of the blood flow are generated and visually shown with the corresponding parameters using Maple software. The Nusselt number and skin friction are introduced in tabular format, with a subsequent thorough discussion.

## 2. Mathematical Formulation

This section will provide a comprehensive overview of the research methodology employed in this study, followed by the generation of problem formulations aided by visual representations grounded in physical problem scenarios.

### 2.1. Research methodology

In this context, the Navier-Stokes equation in cylindrical coordinates is employed to develop the governing equations for momentum and energy. The governing equations that have been derived are expressed in the form of partial differential equations (PDEs) and linear equation. The initial stage involves the dimensionalization process, wherein the dimensionless variables and nanofluid thermophysical properties are substituted into the governing equations and their associated conditions. The primary goal of this technique is to obtain a dimensionless formulation of the governing equation together with the associated conditions by eliminating the units that are inherent in the governing equations. Through the process of dimensionalization, the study yields dimensionless parameters, including the Darcy number, magnetic parameter, Grashof number, and Prandtl number. These parameters are significant because they require detailed analysis and graphical representation. Table 1 displays example of the dimensionless parameter derived through the elimination of dimensional units. A concise evaluation of the latest technology, applications, or products is presented.

Table 1. Example of dimensionless parameters.

Parameters	Dimensional Units
Electrical conductivity, $\sigma$	$[T^3][I^2][M^{-1}][L^{-3}]$
Radius of cylinder, $r_0$	$[L]$
Applied magnetic field, $B_0$	$[M][T^2][I]$
Dynamic viscosity, $\mu$	$[M][L^{-1}][T^{-1}]$
Magnetic parameter, $M$	$M = \frac{\sigma r_0^2 B_0^2}{\mu} = \frac{[T^3][I^2][L^2][M^2][L][T]}{[M][L^3][T^2][I^2][M]} = 1$





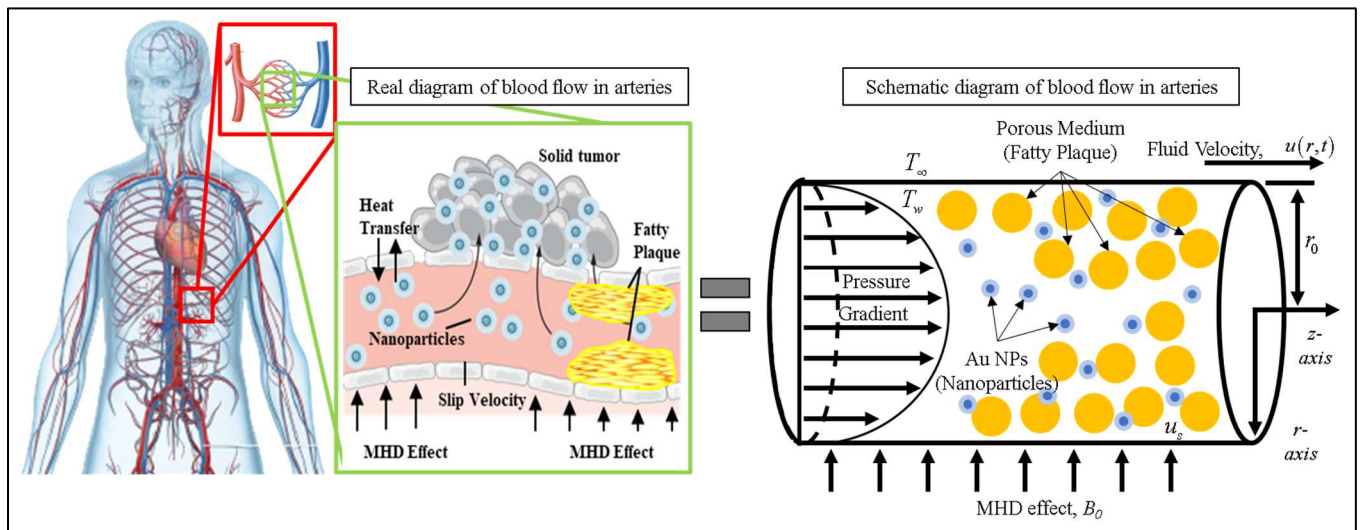


Fig. 1. The structural context of the fluid flow scenario [76–78].

Subsequently, the governing equations in the partial differential equation (PDE) and dimensionless forms are reduced into ordinary differential equation (ODE) form by employing the combination of Laplace transform and finite Hankel transform techniques. Both techniques are highly effective tools for solving the linear equation problem analytically in terms of both time and radial coordinates. By employing these techniques, the solution is derived for the nanofluid velocity and temperature in terms of transformation variables, specifically  $r_n$  and  $s$ . Then, the inverse Laplace transform and the inverse finite Hankel transform are employed to revert the governing equations of the nanofluid’s velocity and temperature back to their original domains, namely the variables  $r$  and  $t$ . Consequently, this analytical approach yields the solutions for nanofluid velocity and temperature. Finally, the analytical solutions for the temperature and velocity of the nanofluid are plotted and evaluated with Maple software, incorporating dimensionless parameters and other relevant constant constants. The Maple software is well-suited for the analytical solution and direct plotting of mathematical problems. To generate plots, we employ simulated data derived from prior research closely aligned with the specific physical application.

**2.2. Problem formulation**

The incompressibility of human blood which dispersed with the gold nanoparticles (AuNPs) as it circulates through the small arteries is a subject of consideration. This study explores the flow characteristics of a Casson fluid containing AuNPs within a cylindrical region defined by a radius of  $r_0$ . The  $z$ -axis is indicative of the direction in which the Casson fluid experiences motion along the axis, while the  $r$ -axis is perpendicular to the  $z$ -axis. The blood motion is due to pulsatile flow caused by the heart’s beating action and convection flow in the cylinder. The applied magnetic field,  $B_0$  is engaged uniformly along the  $r$ -axis, and all the induced magnetic and viscous dissipation is disregarded. This study is examining the impact of the porous medium, which represents fatty plaque or blood clots. Moreover, slippage occurs between blood flow and the solid arteries, which is taken into account. Let us consider the variables  $r$  and  $t$  as the exclusive constituents of the blood’s velocity and temperature, respectively. The issue is physically described in Fig. 1.

The constitutive equation that governs the relationship between shear stress and strain rate for an incompressible flow of a Casson fluid is expressed as follows [79, 80]:

$$\tau_{ij} = \begin{cases} 2 \left( \mu_B + \frac{\tau_y}{\sqrt{2\pi}} \right) e_{ij}; & \pi > \pi_c, \\ 2 \left( \mu_B + \frac{\tau_y}{\sqrt{2\pi_c}} \right) e_{ij}; & \pi < \pi_c, \end{cases} \tag{1}$$

where  $\pi = e_{ij}e_{ij}$  and  $e_{ij}$  are the  $(i,j)$ -th constituent of the deformation rate,  $\mu_B$  is the plastic dynamic viscosity,  $\tau_y$  is the fluid yield stress,  $\pi$  is a product of the deformation rate and itself,  $\pi_c$  is a critical value of this product based on the non-Newtonian model. This study centers its attention on the Casson fluid model instead of the Papanastasiou-Casson regularization model. The Papanastasiou-Casson regularisation model is a newer approach than the Casson fluid model. Therefore, validating the current findings has become easier due to the extensive research conducted on the Casson fluid model over the past few decades. Besides that, the Casson fluid model is simpler than the Papanastasiou-Casson regularisation model. Numerous researchers have conducted numerical investigations the Papanastasiou-Casson regularisation model due to its complexity [81]. Since current study focus on the analytical solution, it is important to consider the Casson fluid model. According to Boussinesq’s approximation, the Tiwari and Das nanofluid model, and the above presumptions, the governing equations of the present problem can be presented as [64, 82]:

$$\rho_{nf} \frac{\partial u^*(r,t)}{\partial t^*} = -\frac{\partial p^*}{\partial z^*} + \mu_{nf} \left( 1 + \frac{1}{\beta} \right) \left( \frac{\partial^2 u^*(r,t)}{\partial r^{*2}} + \frac{1}{r^*} \frac{\partial u^*(r,t)}{\partial r^*} \right) - \sigma_{nf} B_0^2 u^*(r,t) - \frac{\mu_{nf}}{k_p} u^*(r,t) + g(\rho\beta_T)_{nf} (T - T_\infty), \tag{2}$$

$$(\rho c_p)_{nf} \frac{\partial T}{\partial t^*} = k_{nf} \left( \frac{\partial^2 T}{\partial r^{*2}} + \frac{1}{r^*} \frac{\partial T}{\partial r^*} \right), \tag{3}$$



**Table 2.** Nanofluid thermophysical properties [83].

Nanofluid Properties	Equations
Effective density, $\rho_{nf}$	$\rho_{nf} = (1 - \phi)\rho_f + \phi\rho_s$
Effective dynamic viscosity, $\mu_{nf}$	$\mu_{nf} = \frac{\mu_f}{(1 - \phi)^{2.5}}$
Effective electrical conductivity, $\sigma_{nf}$	$\sigma_{nf} = \sigma_f \left[ 1 + \frac{3(\sigma - 1)\phi}{(\sigma + 2) - (\sigma - 1)\phi} \right], \sigma = \frac{\sigma_s}{\sigma_f}$
Effective thermal expansion coefficient, $(\rho\beta_T)_{nf}$	$(\rho\beta_T)_{nf} = (1 - \phi)(\rho\beta_T)_f + \phi(\rho\beta_T)_s$
Effective heat capacity coefficient, $(\rho C_p)_{nf}$	$(\rho C_p)_{nf} = (1 - \phi)(\rho C_p)_f + \phi(\rho C_p)_s$
Effective thermal conductivity, $k_{nf}$	$k_{nf} = k_f \left[ \frac{k_s + 2k_f - 2\phi(k_f - k_s)}{k_s + 2k_f + \phi(k_f - k_s)} \right]$

where  $u^*$  indicates the velocity component along the z-axis,  $t^*$  indicates the time parameter,  $\partial p^* / \partial z^*$  indicates a pulsatile pressure gradient,  $\beta = \mu_B \sqrt{2\pi_c} / \tau_y$  indicates a non-Newtonian Casson parameter,  $B_0$  indicates applied magnetic field strength,  $k_p$  indicates permeability constant,  $g$  indicates gravitational acceleration,  $T$  indicates the fluid temperature,  $T_\infty$  indicates ambient temperature. Furthermore, the thermophysical properties associated with Casson nanofluids are presented in Table 2 [83].

In Table 2, the subscript symbols  $f, s$  and  $nf$  indicate base fluid, nanoparticles solid, and nanofluid, respectively. Besides,  $\phi$  indicates nanoparticle volume fraction. The present study employed the Maxwell model, which only considers a spherical form of nanoparticles since it is suitable for heat transfer improvement. The nanofluid's viscosity is roughly equivalent to that of the base fluid containing spherical nanoparticles, which are emphasised by Brinkman [84]. When  $t^* = 0$ , both the fluid and the cylinder are in their resting states. Then, the fluid begins to move at the same slip velocity that exists at the boundary as  $t^* > 0$ . The cylinder's temperature simultaneously rises from  $T_\infty$  to the boundary temperature  $T_w$  and then stays constant. The initial and boundary conditions are given as [85, 86]:

$$\begin{aligned} u^*(r^*, 0) = 0 & \quad T^*(r^*, 0) = T_\infty & ; r \in [0, r_0], \\ u^*(r_0^*, t^*) = u_s^* & \quad T^*(r_0^*, t^*) = T_w & ; t^* > 0, \end{aligned} \tag{4}$$

where  $u_s^*$  is the slip velocity condition. The relevant dimensionless variables are stated as [85–87]:

$$t = \frac{t^* \nu}{r_0^2}, \quad r = \frac{r^*}{r_0}, \quad u = \frac{u^*}{u_0}, \quad u_s = \frac{u_s^*}{u_0}, \quad z = \frac{z^*}{r_0}, \quad p = \frac{p^* r_0}{\mu u_0}, \quad \theta = \frac{T - T_\infty}{T_w - T_\infty}. \tag{5}$$

The dimensionless form of PDEs is obtained by transforming the governing Eqs. (2), (3), and conditions (4) with the appropriate dimensionless variables, which gain as:

$$\frac{\partial u(r, t)}{\partial t} = -b_5 \frac{\partial p}{\partial z} + b_6 \beta_1 \left( \frac{\partial^2 u(r, t)}{\partial r^2} + \frac{1}{r} \frac{\partial u(r, t)}{\partial r} \right) - \frac{b_6}{Da} u(r, t) - b_8 M u(r, t) + b_9 Gr \theta(r, t), \tag{6}$$

$$\frac{\partial \theta(r, t)}{\partial t} = \frac{b_3}{Pr} \left( \frac{\partial^2 \theta(r, t)}{\partial r^2} + \frac{1}{r} \frac{\partial \theta(r, t)}{\partial r} \right), \tag{7}$$

and the conditions:

$$\begin{aligned} u(r, 0) = 0, & \quad \theta(r, 0) = 0 & ; r \in [0, 1], \\ u(1, t) = u_s, & \quad \theta(1, t) = 1 & ; t > 0, \end{aligned} \tag{8}$$

where the constant parameters are:

$$\begin{aligned} b_5 &= \frac{1}{(1 - \phi) + \frac{\phi \rho_s}{\rho_f}}, \quad b_6 = \frac{b_5}{(1 - \phi)^{2.5}}, \quad b_8 = b_4 b_5, \quad b_4 = 1 + \frac{3(\sigma - 1)\phi}{(\sigma + 2) - (\sigma - 1)\phi}, \quad \sigma = \frac{\sigma_s}{\sigma_f}, \quad b_9 = b_5 b_7, \quad b_7 = (1 - \phi) + \frac{\phi(\rho\beta_T)_s}{(\rho\beta_T)_f}, \\ b_3 &= \frac{b_1}{b_2}, \quad b_1 = \frac{k_s + 2k_f - 2\phi(k_f - k_s)}{k_s + 2k_f + \phi(k_f - k_s)}, \quad b_2 = (1 - \phi) + \frac{\phi(\rho C_p)_s}{(\rho C_p)_f}, \quad \beta_1 = \frac{1}{\beta_0}, \quad \beta_0 = 1 + \frac{1}{\beta}. \end{aligned}$$

From the dimensionalization process, the obtained dimensionless parameters are as follows; Darcy number  $Da = k_p / r_0^2$ , magnetic parameter  $M = \sigma_f r_0^2 B_0^2 / \mu_f$ , Grashof number  $Gr = g(\beta_T)_f (T_w - T_\infty) r_0^2 / \nu_f u_0$  and Prandtl number  $Pr = \nu_f (\rho C_p)_f / k_f$ . Moreover,  $-\partial p / \partial z = A_0 + A_1 \cos(\omega t)$  indicates the pulsatile pressure gradient that imitates the heart's pumping movement [88], where  $A_0$  and  $A_1$  are the constants of pulsatile amplitude, and  $\omega$  is a pulsatile frequency. It is possible to rewrite the dimensionless momentum governing equation as:

$$\frac{\partial u(r, t)}{\partial t} = b_5 (A_0 + A_1 \cos(\omega t)) + b_6 \beta_1 \left( \frac{\partial^2 u(r, t)}{\partial r^2} + \frac{1}{r} \frac{\partial u(r, t)}{\partial r} \right) - \frac{b_6}{Da} u(r, t) - b_8 M u(r, t) + b_9 Gr \theta(r, t). \tag{9}$$



### 3. Problem Solution

Evaluating blood flow within the slipping cylinder containing AuNPs requires the application of integrated techniques that combine the Laplace and finite Hankel transforms. When dealing with cylindrical domains, the finite Hankel transform offers valuable benefits, while the Laplace transform is helpful for initial-boundary values and transient concerns. The ODEs result from the reduction of the PDEs. By applying the inverse for both transformations, the analytical results will be attained.

#### 3.1. Calculation of temperature

Firstly, the dimensionless form of the energy governing Eq. (7) together with the dimensionless conditions (8) employ the Laplace transform technique, which yields:

$$s\bar{\theta}(r,s) = \frac{b_3}{Pr} \left[ \frac{d^2\bar{\theta}(r,s)}{dr^2} + \frac{1}{r} \frac{d\bar{\theta}(r,s)}{dr} \right], \quad (10)$$

$$\bar{\theta}(1,s) = \frac{1}{s}, \quad (11)$$

where  $\bar{\theta}(r,s)$  indicates the Laplace transform of the function  $\theta(r,t)$ , and the transformation variable is  $s$ . Secondly, Eq. (10) is transformed by using the finite Hankel transform of zero-order together with the condition (11) to produce:

$$\bar{\theta}_H(r_n,s) = b_3 \frac{r_n J_1(r_n)}{s} \left[ \frac{1}{sPr + b_3 r_n^2} \right], \quad (12)$$

where  $\bar{\theta}_H(r_n,s) = \int_0^1 r \bar{\theta}(r,s) J_0(rr_n) dr$  is the finite Hankel transform of the function  $\bar{\theta}(r,s)$  and  $r_n$  with  $n = 0, 1, \dots$  are the positive roots of the equation  $J_0(x) = 0$  where  $J_0$  is the Bessel function of the first kind and zero-order, and  $J_1$  is the Bessel function of the first kind and first-order. Then, the result of simplifying Eq. (12) is:

$$\bar{\theta}_H(r_n,s) = \frac{J_1(r_n)}{r_n} \left[ \frac{1}{s} - \frac{1}{s + b_3 r_n^2 / Pr} \right]. \quad (13)$$

Thirdly, Eq. (13) is subjected to the inverse Laplace transform, obtaining as:

$$\theta_H(r_n,t) = \frac{J_1(r_n)}{r_n} \left[ 1 - \exp\left(-\frac{b_3 r_n^2}{Pr} t\right) \right]. \quad (14)$$

Finally, the inverse finite Hankel transform is used to solve the equation analytically for the temperature profiles (14) and is attained as:

$$\theta(r,t) = 1 - 2 \sum_{n=1}^{\infty} \frac{J_0(r_n)}{r_n J_1(r_n)} \exp\left(-\frac{b_3 r_n^2}{Pr} t\right). \quad (15)$$

#### 3.2. Calculation of velocity

The dimensionless momentum equation (9) and the associated conditions (8) are both solved by using the Laplace transform, which results in

$$s\bar{u}(r,s) = b_5 \left( \frac{A_0}{s} + \frac{A_1 s}{s^2 + \omega^2} \right) + b_6 \beta_1 \left[ \frac{d^2\bar{u}(r,s)}{dr^2} + \frac{1}{r} \frac{d\bar{u}(r,s)}{dr} \right] - \frac{b_6}{Da} \bar{u}(r,s) - b_8 M \bar{u}(r,s) + b_9 Gr \bar{\theta}(r,s), \quad (16)$$

$$\bar{u}(1,s) = \frac{u_s}{s}, \quad (17)$$

where  $\bar{u}(r,s)$  is the Laplace transform of the function  $u(r,t)$ . Following that, the method of finite Hankel transform of zero-order is employed to convert Laplace's partial differential equation (16) into an ordinary differential equation (ODE), denoted as:

$$\bar{u}_H(r_n,s) = b_5 \frac{J_1(r_n)}{r_n} \left( \frac{A_0}{s} + \frac{A_1 s}{s^2 + \omega^2} \right) + b_6 \beta_1 r_n J_1(r_n) \frac{u_s}{s} + b_9 Gr \bar{\theta}_H(r_n,s) \left( \frac{1}{s + b_{11}[n]} \right), \quad (18)$$

where  $\bar{u}_H(r_n,s) = \int_0^1 r \bar{u}(r,s) J_0(rr_n) dr$  is the finite Hankel transform of the function  $\bar{u}(r,s)$  and  $b_{11}[n] = b_{10} + b_6 \beta_1 r_n^2$ ,  $b_{10} = b_6 / Da + b_8 M$  are the constant parameters. Subsequently, Eq. (18) is subjected to the inverse Laplace transform, yielding as:

$$u_H(r_n,t) = \frac{J_1(r_n)}{r_n} [f_1(r_n,t) + f_2(r_n,t) + f_3(r_n,t) + f_4(r_n,t)], \quad (19)$$

where

$$f_1(r_n,t) = u_s \left[ 1 + \exp(-b_{11}[n]t) \left( \frac{b_{10}}{b_{11}[n]} - 1 \right) - \frac{b_{10}}{b_{11}[n]} \right],$$



$$f_2(r_n, t) = \frac{b_5 A_0}{b_{11} [n]} (1 - \exp(-b_{11} [n]t)),$$

$$f_3(r_n, t) = \frac{A_1 b_5}{\omega^2 + b_{11}^2 [n]} (\omega \sin(\omega t) + b_{11} [n] \cos(\omega t) - b_{11} [n] \exp(-b_{11} [n]t)),$$

$$f_4(r_n, t) = b_9 Gr \left[ \frac{1}{b_{11} [n]} - \exp(-b_{11} [n]t) \left( \frac{1}{b_{11} [n]} - \frac{Pr}{Pr b_{11} [n] - b_3 r_n^2} \right) - \frac{Pr \exp\left(-\frac{b_3 r_n^2 t}{Pr}\right)}{Pr b_{11} [n] - b_3 r_n^2} \right].$$

The inverse finite Hankel transform is then used to solve Eq. (19), which is denoted as the analytical solution of the velocity profile, which is written as:

$$u(r, t) = u_s + 2u_s \sum_{n=1}^{\infty} \frac{J_0(r r_n)}{r_n J_1(r_n)} \exp(-b_{11} [n]t) \left( \frac{b_{10}}{b_{11} [n]} - 1 \right) - 2u_s \sum_{n=1}^{\infty} \frac{J_0(r r_n)}{r_n J_1(r_n)} \frac{b_{10}}{b_{11} [n]} + 2A_0 b_5 \sum_{n=1}^{\infty} \frac{J_0(r r_n)}{r_n J_1(r_n)} \left( \frac{1 - \exp(-b_{11} [n]t)}{b_{11} [n]} \right) + 2A_1 b_5 \sum_{n=1}^{\infty} \frac{J_0(r r_n)}{r_n J_1(r_n)} \left( \frac{\omega \sin(\omega t) + b_{11} [n] \cos(\omega t) - b_{11} [n] \exp(-b_{11} [n]t)}{\omega^2 + b_{11}^2 [n]} \right) + 2Gr b_9 \sum_{n=1}^{\infty} \frac{J_0(r r_n)}{r_n J_1(r_n)} \left[ \frac{1}{b_{11} [n]} + \frac{b_3 r_n^2 \exp(-b_{11} [n]t)}{b_{11} [n] (Pr b_{11} [n] - b_3 r_n^2)} - \frac{Pr \exp\left(-\frac{b_3 r_n^2 t}{Pr}\right)}{Pr b_{11} [n] - b_3 r_n^2} \right]. \tag{20}$$

### 4. Result and Discussion

The current investigation addresses the issue of pulsatile flow in Casson nanofluid under the influence of magnetohydrodynamics, slip, porosity, and convective heat transfer. The problem is resolved through the application of the Laplace transform and the finite Hankel transform. The velocity and temperature profiles were graphically visualised with respect to the corresponding parameters such as Casson parameter  $\beta$ , magnetic parameter  $M$ , Darcy number  $Da$ , Grashof number  $Gr$ , Prandtl number  $Pr$ , slip velocity parameter  $u_s$ , nanoparticle volume fraction parameter  $\phi$  and time parameter  $t$ . The parameters applied in this study to plot the graph are as follows;  $t = 0.6$  represents the earlier phase,  $t = 5.0$  represents the equilibrium phase,  $Pr = 21.0$  represents human blood,  $u_s = 0$  represents no-slip effect,  $A_0 = A_1 = 0.05$  represents blood flow in a blood vessel [89] and  $\omega = \pi / 4$ ,  $\beta = 0.4, 0.8, 1.2$ ,  $\phi = 0.0, 0.02, 0.04$  [64, 85, 88]. Besides, some parameters are estimated to obtain wide-range graphs such as  $Pr = 10, 15, 21$ ,  $Gr = Da = 1.0, 2.0, 3.0$ ,  $M = 0.0, 1.0, 2.0$  and  $u_s = 0.2$  represents slip effect. Furthermore, Table 3 contains the constant values of the thermophysical properties of nanofluids [64, 82].

Additionally, the present result as in equation (20) is validated by comparing it with the previous studies by Khan et al. [86] and Imtiaz et al. [64]. First limiting case is employed by allowing the present result and previous study Khan et al. [86] with  $\beta = Da = \infty$ ,  $u_s = 1.0$ ,  $A_0 = A_1 = M = \phi = \omega = 0$ . Second limiting case is applied between present study and previous study Imtiaz et al. [64] by letting  $Da = \infty$  and  $u_s = 1.0$ . The observation shows that the graphs are aligned, which means the present result is accurate, as displayed in Figs. 2a and 2b.

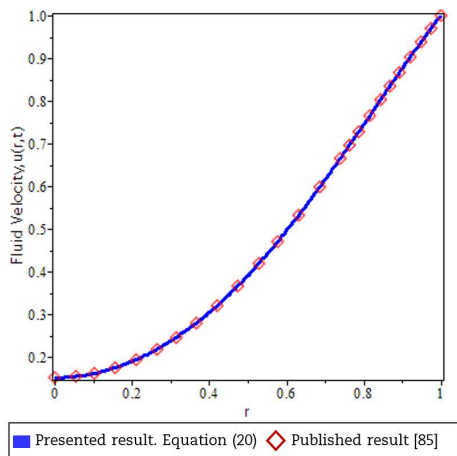


Fig. 2a. Comparative analysis between present result, equation (20) and Khan et al. [85].

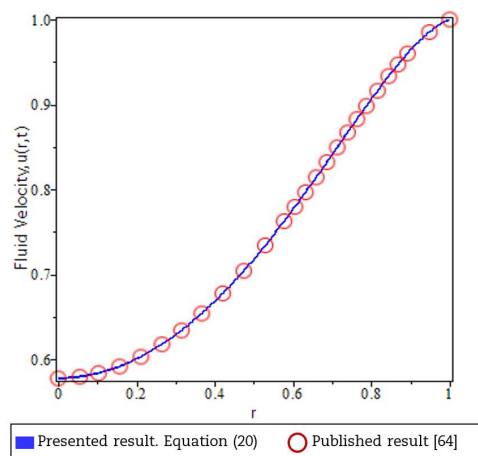


Fig. 2b. Comparative analysis between present result, equation (20) and Imtiaz et al. [64].

Table 3. Nanofluid thermophysical properties constant values.

Properties material	Blood (fluid)	Gold (solid)
$\rho$ (Kg/m <sup>3</sup> )	1063	19300
$C_p$ (J/KgK)	3594	129
$k$ (W/mK)	0.492	318
$\beta_T \times 10^{-5}$ (1/K)	0.18	1.4
$\sigma$ (S/m)	0.8	$4.1 \times 10^7$





Figure 3 illustrates the variation of the fluid velocity under the influence of slip velocity, as well as in its absence, as evidenced by the changes in the Casson parameter  $\beta$ . Generally, Casson fluid behavior mimics human blood flow via small arteries [88]. The graph for the small-time interval at  $t = 0.6$  reflects that when  $\beta$  rises, blood nanofluid flow near the boundary increases and decreases as it flows towards the cylinder's center in both cases. This phenomenon occurs because the fluid yield stress decreases in close proximity to the boundary, and only a small force is needed to initiate the flow. However, internal friction increases as blood nanofluid flows towards the center, which leads to a decrease in blood nanofluid flow. Besides, as time increases at  $t = 5.0$ , the blood nanofluid flow declines with the increment of  $\beta$  for both presence and absence of slip velocity conditions. The rationale for this phenomenon is that an augmentation in  $\beta$  results in a corresponding augmentation in the dynamic viscosity of the fluid. It causes the shear thickening factor to rise and slow down the blood nanofluid flow.

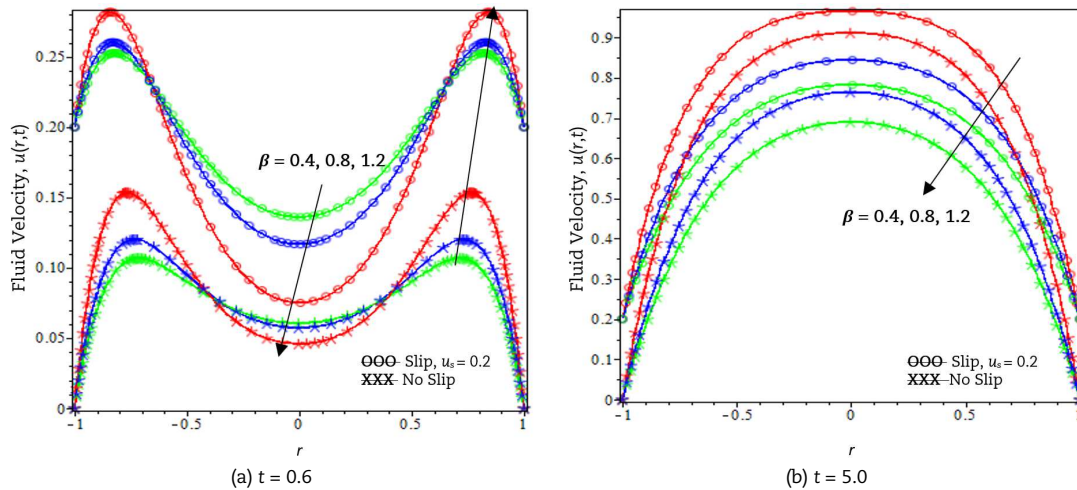


Fig. 3. Casson parameters influence on velocity profiles  $u(r,t)$  when  $A_0=A_1=0.05$ ,  $\omega=\pi/4$ ,  $M=Da=Gr=1$ ,  $Pr=21$ ,  $\phi=0.02$ .

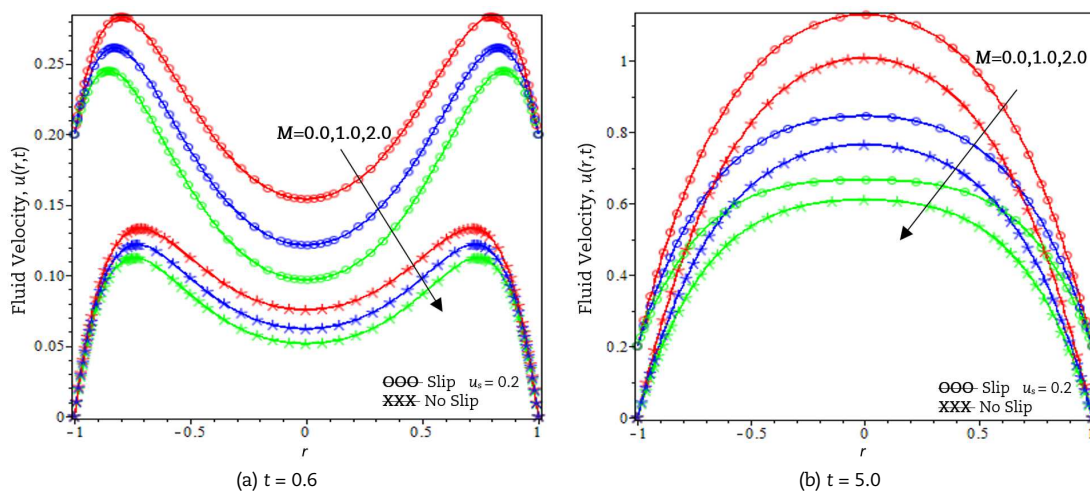


Fig. 4. Magnetic parameters influence on velocity profiles  $u(r,t)$  when  $A_0=A_1=0.05$ ,  $\omega=\pi/4$ ,  $\beta=0.8$ ,  $Da=Gr=1$ ,  $Pr=21$ ,  $\phi=0.02$ .

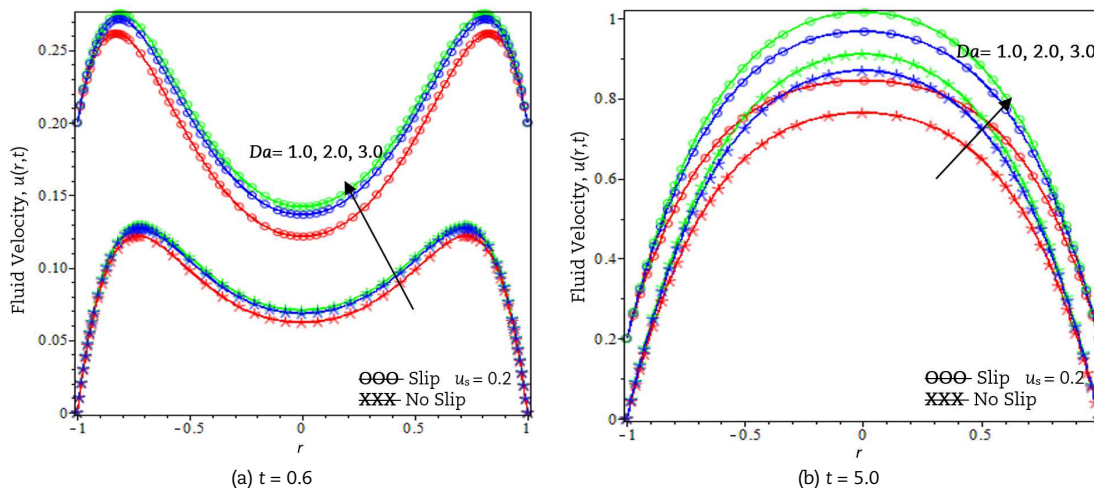


Fig. 5. Darcy number influence on velocity profiles  $u(r,t)$  when  $A_0=A_1=0.05$ ,  $\omega=\pi/4$ ,  $\beta=0.8$ ,  $M=Gr=1$ ,  $Pr=21$ ,  $\phi=0.02$ .





For both cases of slip and no-slip conditions, the velocity of blood in the presence of nanoparticles exhibits a decrease as the magnetic parameter  $M$  increases. at  $t = 0.6$  and  $t = 5.0$  as presented in Fig. 4. The phenomenon arises due to the resistive force, commonly known as the Lorentz force, it acts counter to the blood flow. It is created when the induced current produced by blood flow, which acts as an electrically conducting fluid, interacts with the magnetic field and results in a decline in blood flow. Although blood flow is influenced by strong magnetic fields like magnetic resonance imaging (MRI), it can also be influenced by weak magnetic fields, which exist in the cardiovascular system and with additional external electronic devices like TVs and phones.

Figure 5 depicts blood behavior under the influence of a porous medium with slip and no-slip effects. The porous medium represents Darcy number  $Da$ . Based on the graph observation, at  $t = 0.6$ , blood flow with nanoparticles slightly rises with the increment of the Darcy number. But at  $t = 5.0$ , the blood flow upsurge with the growth of Darcy number. This is because a higher Darcy number causes porous media to have higher permeability. Thus, larger blood flows with nanoparticles can transmit through the porous medium. It means that there is less risk of blood clots or cholesterol plaques occurring in the blood vessel since blood with nanoparticles can flow smoothly.

Figure 6 illustrates the impact of the pulsatile pressure gradient on the fluid velocity. The steady amplitude,  $A_0$ , and oscillating velocity amplitude,  $A_1$ , are considered the same to denote the flow type of blood flow in the arteries [89]. Based on the graph observation, blood nanofluid flow is obviously growing by increasing the pulsatile pressure gradient for both slip and no-slip conditions at  $t = 0.6$ . This is because it is defined as the heart's beating action, which helps the human blood move faster through the human blood vessel system. Moreover, at  $t = 5.0$ , velocity profiles slightly increase since the system reaches equilibrium. Pulsatile pressure gradients can be regulated to prevent or treat diseases such as hypertension, which is caused by blockage of blood flow.

Figure 7 illustrates the changes in human blood flow behaviour concerning the Grashof number  $Gr$  by having both slip and no-slip effects. According to the graph, the velocity of blood in the presence of nanoparticles exhibits an increase as the  $Gr$  increases. when  $t = 0.6$  and  $t = 5.0$ . The Grashof number is essential when involved with the free convection flow. This refers to the dimensionless quantity that reveals the relationship between buoyancy force and viscosity force exerted on a fluid. It takes place naturally when there is a change in fluid density due to temperature differences. For example, warm fluid will rise due to the buoyancy force, while viscous forces resist the buoyancy force. The buoyancy force upsurge as Grashof number grows. It causes human blood flow to rise. In other words, the temperature gradient in the human body exists due to the thermal regulation mechanisms in the body to sustain the tissue's temperature, which can affect blood flow by altering its viscosity and plasticity.

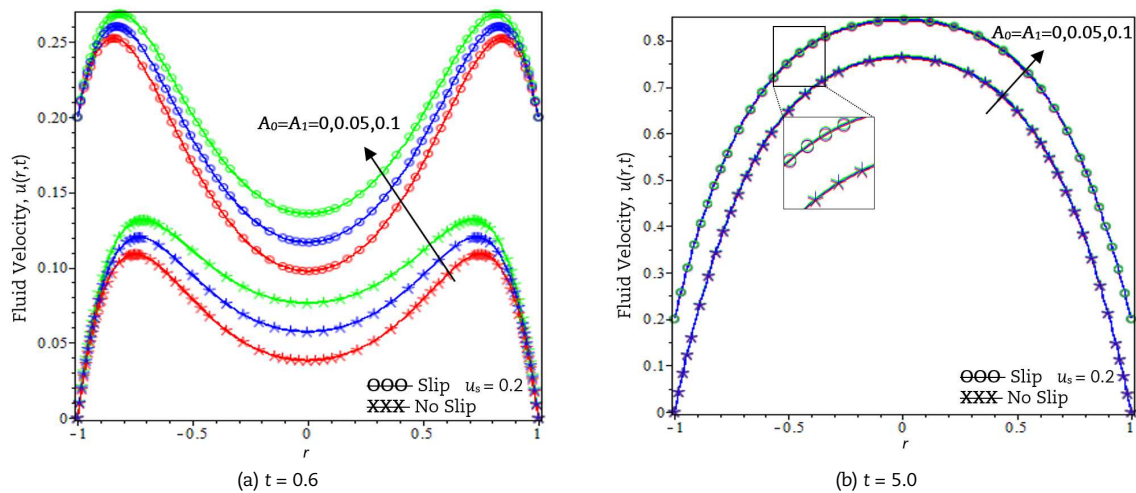


Fig. 6. Amplitude of pulsatile pressure gradient influence on velocity profiles  $u(r,t)$  when  $\omega=\pi/4, \beta=0.8, Da=M=Gr=1, Pr=21, \phi=0.02$ .

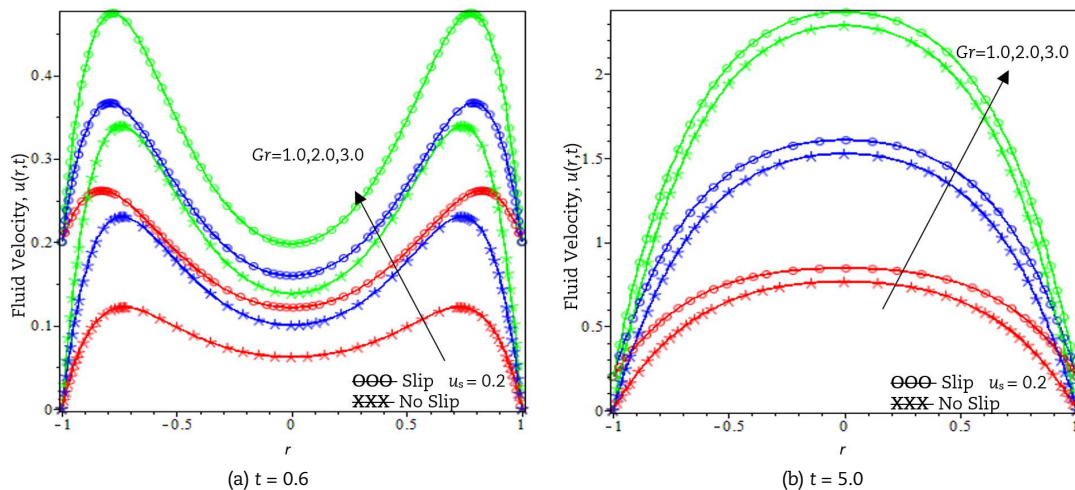


Fig. 7. Grashof number influence on velocity profiles  $u(r,t)$  when  $A_0=A_1=0.05, \omega=\pi/4, \beta=0.8, M=Da=1, Pr=21, \phi=0.02$ .



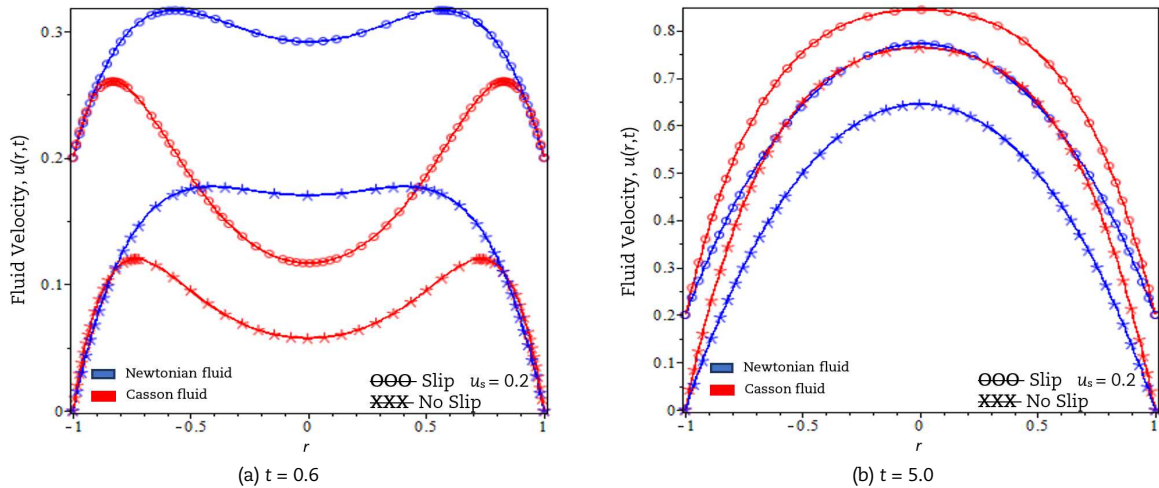


Fig. 8. Comparison of velocity profiles  $u(r,t)$  between Casson fluid and Newtonian fluid when  $A_0=A_1=0.05$ ,  $\omega=\pi/4$ ,  $Gr=M=Da=1$ ,  $\phi=0.02$ .

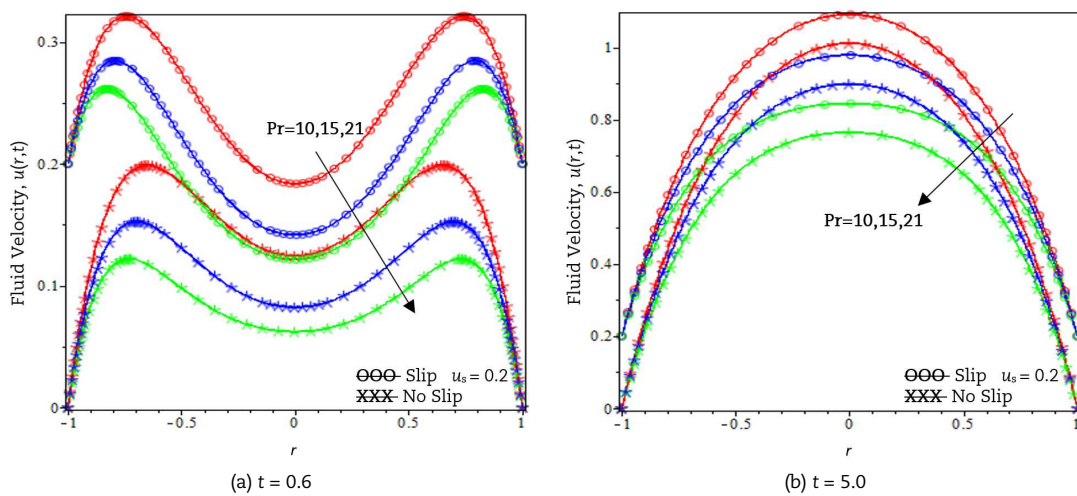


Fig. 9. Prandtl number influence on velocity profiles  $u(r,t)$  when  $A_0=A_1=0.05$ ,  $\omega=\pi/4$ ,  $\beta=0.8$ ,  $Gr=M=Da=1$ ,  $\phi=0.02$ .

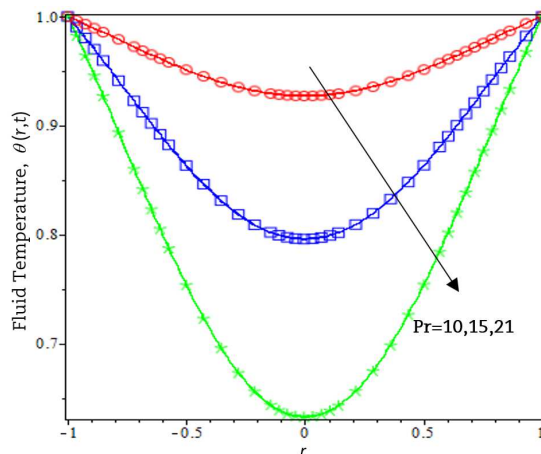


Fig. 10. Prandtl number influence on temperature profiles  $\theta(r,t)$  when  $\phi=0.02$ ,  $t=5.0$ .

Figure 8 presents a comparative analysis of the behaviors exhibited by Casson nanofluid and Newtonian nanofluid, accounting for the effects of slip and no-slip velocities. As  $\beta \rightarrow 0$ , the yield stress characteristic of the Casson parameter tends toward zero, signifying a transition to Newtonian-like fluid behavior. Conversely, when  $\beta \rightarrow 0$ , the non-Newtonian features become more prominent. At  $t = 0.6$ , both nanofluids exhibit concurring velocities in proximity to the boundary of the cylinder, regardless of the slip or no-slip conditions. However, as the center of the cylinder is approached, the velocity of the Casson nanofluid becomes lower than that of the Newtonian nanofluid. This discrepancy can be attributed to the higher viscosity of the Casson nanofluid, resulting in a decelerated fluid flow. Upon reaching  $t = 5.0$ , the velocity of the Casson nanofluid surpasses that of the Newtonian nanofluid in both slip and no-slip scenarios. The velocity boundary layer thickness of Casson fluids is greater than that of Newtonian fluids due to the plastic behaviour exhibited by Casson fluids. Consequently, leading to elevated velocities over extended time intervals.



In the meantime, the influence of Prandtl number  $Pr$  on blood velocity and blood temperature can be seen in Figs. 9 and 10. It is clearly shown in Fig. 9 that as  $Pr$  increases, blood velocity declines for both cases of slip velocity at  $t = 0.6$  and  $t = 5.0$ . This is owing to the fact that  $Pr$  is directly proportional to momentum diffusivity. Momentum diffusivity increases lead to an increase of viscous force, which resists the motion of the nanofluid. It causes a decrement in blood velocity. Moreover, the reduction of blood temperature is observed to be inversely proportional to the increase in  $Pr$ , as depicted in Fig. 10. Thermal diffusivity is inversely proportional to  $Pr$ . Larger  $Pr$  causes quick heat diffusion, and blood temperature decreases.

Figure 11 displays how blood behaviour reacts with variations in nanoparticle volume fraction  $\phi$  for both cases of slip and no-slip effects. When  $\phi = 0$ , it indicates pure human blood. Based on the graph findings, blood flow with nanoparticles is higher than pure blood flow. It also describes that blood velocity increases as  $\phi$  increases for both slip cases when  $t = 0.6$  and  $t = 5.0$ . It is supported by some studies reviewed by Tripathi et al. [90]. Besides, Fig. 12 exhibits blood temperature rise as  $\phi$  grows. Generally, gold nanoparticle has the highest thermal conductivity and is efficient at conducting heat. Upon dispersion within the bloodstream, gold nanoparticles elicit a rise in blood temperature resulting from an increase in heat transfer. The occurrence of the temperature gradient in the blood flow results in a density gradient, which is known as a convective phenomenon. Blood nanoparticles will move from hot to cold until they achieve temperature equilibrium. Hence, the movement of the blood nanoparticles increases when thermal conductivity increases. A similar pattern of velocity and temperature profiles can be observed within [82].

Figures 3 to 9 and Fig. 11 present the differences in blood flow behaviour between slip and no-slip effects at  $t = 0.6$  and  $t = 5.0$ . As we can see, the amplitude of blood velocity is significantly increased in flow with slip conditions. The slip phenomenon, which affects the flow of blood, is clearly observable at the wall of the cylinder with a radius of 1. At time  $t = 0.6$ , there is a reduction in blood flow as it approaches the central region of the cylindrical structure ( $r = 0$ ). It is owing to the greater viscosity at the cylinder's centre. It is also unable to transfer the entire force that occurs at the cylinder's wall to the cylinder's centre. However, blood flow increases as time becomes larger at  $t = 5.0$  since the blood flow system achieves stability. The obtained results highlight the distinctions between slip and no-slip effects. The slip velocity holds significant importance in mathematical modelling due to its relevance to real-world applications, such as the velocity difference between particles in blood flow and the solid boundary of a blood vessel.

Nusselt number with related parameters such as  $t, Pr, \phi$  is tabulated in Table 4. It presents Nusselt number increasing as  $Pr$  increases. It occurs due to the decrement of thermal diffusivity and leads to the decrement of thermal conductivity. As a consequence, it enhances the Nusselt number. Besides, the Nusselt number declines as  $t$  and  $\phi$  rise. It is because fluid thermal conductivity increases with  $\phi$ . Thermal conductivity is inversely proportional to the Nusselt number. Hence, the Nusselt number declines when thermal conductivity increases. A similar result for the Nusselt number can be found in [91, 92].

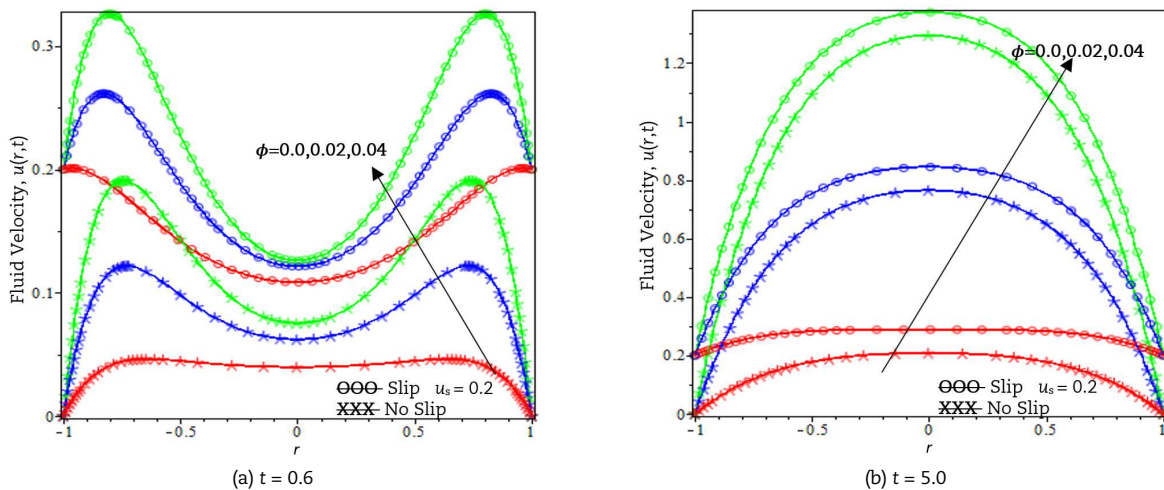


Fig. 11. Nanoparticles volume fraction parameters influence on velocity profiles  $u(r,t)$  when  $A_0=A_1=0.05, \omega=\pi/4, \beta=0.8, M=Da=Gr=1, Pr=21$ .

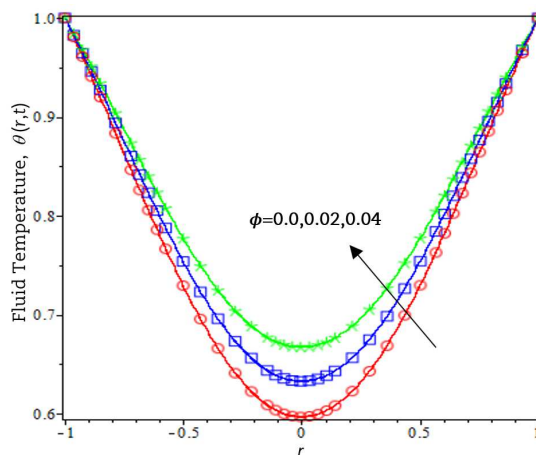


Fig. 12. Nanoparticle volume fraction parameters influence temperature profiles  $\theta(r,t)$  when  $Pr=21, t=5.0$ .



**Table 4.** Nusselt number with various parameters.

t	Pr	$\phi$	Nu	Results
0.50	7.00	0.02	1.519	-
1.00	7.00	0.02	0.864	↓
0.50	21.00	0.02	3.072	↑
0.50	7.00	0.04	1.479	↓

**Table 5.** Skin friction with various parameters.

t	Pr	M	Gr	Da	$\beta$	$u_s$	$\phi$	$\tau$	Results
0.50	7.00	1.00	1.00	1.00	0.80	0.50	0.02	1.346	-
1.00	7.00	1.00	1.00	1.00	0.80	0.50	0.02	2.679	↑
0.50	21.00	1.00	1.00	1.00	0.80	0.50	0.02	0.374	↓
0.50	7.00	2.00	1.00	1.00	0.80	0.50	0.02	0.726	↓
0.50	7.00	1.00	2.00	1.00	0.80	0.50	0.02	4.562	↑
0.50	7.00	1.00	1.00	2.00	0.80	0.50	0.02	1.681	↑
0.50	7.00	1.00	1.00	1.00	1.20	0.50	0.02	0.937	↓
0.50	7.00	1.00	1.00	1.00	0.80	1.00	0.02	-0.651	↓
0.50	7.00	1.00	1.00	1.00	0.80	0.50	0.04	3.456	↑

Table 5 displays the numerical results of the skin friction with different related parameters such as Prandtl number Pr, magnetic parameter M, Grashof number Gr, Darcy number Da, and Casson parameter  $\beta$ , slip velocity  $u_s$ , nanoparticle volume fraction  $\phi$  and time t. Skin friction rises as t, Gr, Da, and  $\phi$  increase. It is due to the increase in the resistance force exerted between fluid moving and an enclosed surface. Besides, skin friction lessens when Pr, M,  $\beta$ , and  $u_s$  increase. It is because resistance forces occur since the fluid velocity decreases.

## 5. Conclusion

In this study, a detailed investigation and analysis of the behaviour of human blood flow in a cylindrical structure in the presence of gold nanoparticles were done. The pulsatile pressure gradient, magnetohydrodynamics (MHD), porosity, slip velocity, and convective heat transfer are factors that exert an influence on blood flow. All the effects considered have an essential role in practical applications, such as pulsatile pressure gradients indicating heart pumping, MHD denoting natural magnetic field, and man-made magnetic field such as handphones, and porosity representing fatty plaque or blood clots. Besides, convection flow exists due to the human body temperature gradient, and slip velocity occurs due to slippage between the blood nanofluid and solid boundary. Hence, the present study obtained significant results effectively in biomedical applications such as nano-cryosurgery (tumour treatment), since experimental studies consume cost and time. The combination methods of the Laplace transform and the finite Hankel transform is being used to analytically solve this problem. The current findings align with the prior research conducted by Khan *et al.* [86], Imtiaz *et al.* [64] and satisfy the imposed boundary conditions. The blood flow behaviour is plotted graphically and analysed with the associated parameters. The results can be deduced as;

For a small-time interval at  $t = 0.6$ , as  $\beta$  increases, blood flow near the cylinder's wall incline but it starts to decline as it approaches the cylinder's centre. When the time interval is larger at  $t = 5.0$ ,  $\beta$  improves blood circulation in both the peripheral and central regions.

- i. The blood flow with nanoparticles increases as Da, Gr,  $u_s$ ,  $\phi$ ,  $A_0$ ,  $A_1$  and t grow.
- ii. Large values of M and Pr cause blood nanofluid velocity to reduce.
- iii. Temperature profiles decrease with Pr but increase with  $\phi$ .
- iv. The influence of slip velocity is evidently observable on the wall of the cylinder.
- v. The Nusselt number rises with Pr but lessens as t and  $\phi$  increase.
- vi. An increment of Gr, Da,  $\phi$ , and t causes an increment of skin friction.
- vii. Meanwhile, decrement in skin friction due to large values of Pr, M,  $\beta$ , and  $u_s$ .

To make the study more realistic, the slip temperature can be considered for future research. Furthermore, it is also possible to take into account the impact of other heat transfer processes involved, such as radiation. Furthering this study is also necessary to consider other practical effects, such as chemical reactions due to the involvement of the drug and the inclined blood vessels. In addition, alternative fluids like Herschel-Bulkley and Jeffrey fluids that simulate blood flow in different scenarios can be considered. Besides that, this problem can be extended by applying Casson- Papanastasiou regularization model in numerical approach in the future.

## Author Contributions

Wan Faezah Wan Azmi prepared the research conceptualization, developed the research methodology, conducted the formal analysis and write the original draft; Ahmad Qushairi Mohamad prepared the research conceptualization, validate the findings, reviewed and edited the writing and provided supervision; Lim Yeou Jiann developed the methodology, utilized the software, reviewed and edited the manuscript; Sharidan Shafie provided supervision and acquired funding.

## Acknowledgments

Not applicable.





## Conflict of Interest

The authors declared no potential conflicts of interest concerning the research, authorship, and publication of this article.

## Funding

The authors would like to acknowledge the financial support from Universiti Teknologi Malaysia for the funding under Others Grant Scheme (R.J130000.7354.4B748) and Matching Grant Scheme (Q.J130000.3054.03M77).

## Data Availability Statements

Not applicable.

## Nomenclature

$\sigma_{nf}$	Nanofluid electrical conductivity [S/m]	$r$	Coordinate axis of the plate
$\sigma_f$	Fluid electrical conductivity [S/m]	$z$	Coordinate axis of the plate
$\sigma_s$	Solid nanoparticles electrical conductivity [S/m]	$\rho_{nf}$	Nanofluid density [kg/m <sup>3</sup> ]
$B_0$	Applied magnetic field [A/m]	$\rho_f$	Fluid density [kg/m <sup>3</sup> ]
$\mu_B$	Non-Newtonian fluid plastic dynamic viscosity [N.s/m <sup>2</sup> ]	$\rho_s$	Solid nanoparticles density [kg/m <sup>3</sup> ]
$\mu_f$	Fluid plastic dynamic viscosity [N.s/m <sup>2</sup> ]	$p$	Pressure [Pa]
$\tau_{ij}$	Component of stress tensor [Pa]	$\mu_{nf}$	Nanofluid dynamic viscosity [N.s/m <sup>2</sup> ]
$\tau_y$	Fluid yield stress [Pa]	$\beta$	Casson fluid parameter
$e_{ij}$	Constituent of the deformation rate [1/s]	$\beta_0, \beta_1$	Constant parameter for Casson fluid
$\pi$	Product of the deformation rate	$k_p$	Permeability [N/A <sup>2</sup> ]
$\pi_c$	Critical values of this product based on non-Newtonian model	$g$	Gravitational acceleration [m/s <sup>2</sup> ]
$u^*$	Velocity component along the z-axis [m/s]	$(\beta_T)_{nf}$	Nanofluid thermal expansion coefficient [1/K]
$t^*$	Time [s]	$T$	Fluid temperature [°C]
$(c_p)_{nf}$	Nanofluid specific heat at constant pressure [J/kg.K]	$T_\infty$	Ambient temperature [°C]
$k_{nf}$	Nanofluid thermal conductivity [W/m.K]	$u_s$	Slip velocity [m/s]
$r_0$	Radius of cylinder [m]	$T_w$	Boundary temperature [°C]
$\nu$	Kinematic viscosity [m <sup>2</sup> /s]	$\phi$	Nanoparticle volume fraction
$Da$	Dimensionless Darcy number	$Gr$	Dimensionless Grashof number
$M$	Dimensionless magnetic parameter	$Pr$	Dimensionless Prandtl number
$\theta$	Dimensionless fluid temperature	$\Omega$	Pulsatile frequency [Hz]
$A_0$	Constant steady pulsatile amplitude [Pa]	$S$	Laplace transformation variable
$A_1$	Constant oscillating pulsatile amplitude [Pa]	$J_0$	Bessel function of the first kind and zero-order
$r_n$	Positive roots of the equation $J_0(x) = 0$	$J_1$	Bessel function of the first kind and first-order
$\tau$	Skin friction	$Nu$	Nusselt number

## References

- [1] Yáñez, C., DeMas-Giménez, G., Royo, S., Overview of Biofluids and Flow Sensing Techniques Applied in Clinical Practice, *Sensors*, 22, 2022, 6836.
- [2] Liepsch, D., Biofluid mechanics, *Biomed. Tech.*, 43, 4, 1998, 94–99.
- [3] Chhabra, R. P., *Non-Newtonian Fluids: An Introduction*, SERC School-cum-Symposium on Rheology of complex fluids, 2010.
- [4] Baieth, H. A. E., Physical parameters of blood as a non-Newtonian fluid, *Int. J. Biomed. Sci.*, 4, 2008, 323–329.
- [5] Windberger, U., Sparer, A., Elsayad, K., The role of plasma in the yield stress of blood, *Clin. Hemorheol. Microcirc.*, 84, 2023, 369–383.
- [6] Wajihah, S. A., Sankar, D. S., A review on non-Newtonian fluid models for multi-layered blood rheology in constricted arteries, *Arch. Appl. Mech.*, 93, 2023, 1771–1796.
- [7] Venkatesan, J., Sankar, D. S., Hemalatha, K., Yatim, Y., Mathematical analysis of Casson fluid model for blood rheology in stenosed narrow arteries, *J. Appl. Math.*, 2013, 2013, 583809.
- [8] Sochi, T., Non-Newtonian flow in porous media, *Polymer*, 51, 2010, 5007–5023.
- [9] Misra, J. C., Adhikary, S. D., Shit, G. G., Mathematical analysis of blood flow through an arterial segment with time-dependent stenosis, *Math. Model. Anal.*, 13, 2008, 401–412.
- [10] Siddiqui, S. U., Verma, N. K., Mishra, S., Gupta, R. S., Mathematical modelling of pulsatile flow of Casson's fluid in arterial stenosis, *Appl. Math. Comput.*, 210, 2009, 1–10.
- [11] Kauffman, R. B., *Thermoregulatory Physiology, Doomsday Preppers and Surviving the Unexpected Emergency*, 2015, 1–4.
- [12] Zolfaghari, A., Maerefat, M., *Bioheat Transfer*, Developments in Heat Transfer, 2011, 153–170.
- [13] Luchakov, Y. I., Nozdrachev, A. D., Mechanism of heat transfer in different regions of human body, *Biol. Bull.*, 36, 2009, 53–57.
- [14] Pop, I., Sheremet, M., Free convection in a square cavity filled with a Casson fluid under the effects of thermal radiation and viscous dissipation, *Int. J. Numer. Methods Heat Fluid Flow*, 27, 2017, 2318–2332.
- [15] Aghighi, M. S., Metivier, C., Masoumi, H., Natural convection of Casson fluid in a square enclosure, *Multidiscip. Model. Mater. Struct.*, 16, 2020, 1245–1259.
- [16] Sheikholeslami, M., Ganji, D. D., *Magnetohydrodynamic and ferrohydrodynamic, External Magnetic Field Effects on Hydrothermal Treatment of Nanofluid*, William Andrew Publishing, Norwich, New York, USA, 2016.
- [17] Scanlon V. C., Sanders, T., *Essentials of Anatomy and Physiology*, FA Davis, 2018.




- [18] Abdalla, S., Al-ameer, S. S., Al-Magaishi, S. H., Electrical properties with relaxation through human blood, *Biomicrofluidics*, 4, 2010, 1–16.
- [19] Uchikawa, Y., Kotani, M., Measurement of Magnetic Field Produced from the Human Body, *IEEE Transl. J. Magn. Japan*, 7, 1992, 600–607.
- [20] Kivrak, E., Yurt, K., Kaplan, A., Alkan, I., Altun, G., Effects of electromagnetic fields exposure on the antioxidant defense system, *J. Microsc. Ultrastruct.*, 5, 2017, 167.
- [21] Keltner, J. R., Roos, M. S., Brakeman, P. R., Budinger, T. F., Magneto-hydrodynamics of blood flow, *Magn. Reson. Med.*, 16, 1990, 139–149.
- [22] Rashidi, S., Esfahani, J. A., Maskaniyan, M., Applications of magneto-hydrodynamics in biological systems-a review on the numerical studies, *J. Magn. Mater.*, 439, 2017, 358–372.
- [23] Ali, F., Imtiaz, A., Khan, I., Sheikh, N. A., Hemodynamic flow in a vertical cylinder with heat transfer: Two-phase caputo-fabrizio fractional model, *J. Magn.*, 23, 2018, 179–191.
- [24] Ali, F., Imtiaz, A., Khan, I., Sheikh, N. A., Flow of magnetic particles in blood with isothermal heating: A fractional model for two-phase flow, *J. Magn. Mater.*, 456, 2018, 413–422.
- [25] Ali, F., Khan, N., Imtiaz, A., Khan, I., Sheikh, N. A., The impact of magneto-hydrodynamics and heat transfer on the unsteady flow of Casson fluid in an oscillating cylinder via integral transform: A Caputo-Fabrizio fractional model, *Pramana - J. Phys.*, 93, 2019, 1–12.
- [26] Kumar, G., Rizvi, S. M., Casson fluid flow past on vertical cylinder in the presence of chemical reaction and magnetic field, *Appl. Appl. Math. An Int. J.*, 16, 2021, 524–537.
- [27] Mehmood, O. U., Mustapha, N., Shafie, S., Unsteady Two-Dimensional Blood Flow in Porous Artery with Multi-Irregular Stenoses, *Transp. Porous Media*, 92, 2012, 259–275.
- [28] Khaled, A. R. A., Vafai, K., The role of porous media in modeling flow and heat transfer in biological tissues, *Int. J. Heat Mass Transf.*, 46, 2003, 4989–5003.
- [29] Omamoke, E., Amos, E., Jatari, E., Impact of Thermal Radiation and Heat Source on MHD Blood Flow with an Inclined Magnetic Field in Treating Tumor and Low Blood, *Asian Res. J. Math.*, 2020, 77–87.
- [30] Dash, R. K., Mehta, K. N., Jayaraman, G., Casson Fluid Flow in a Pipe Filled with a Homogeneous Porous Medium, *Int. J. Engng Sci.*, 34, 1996, 1145–1156.
- [31] Anurag, Singh, A. K., Role of heat source / sink in transient free convective flow through a vertical cylinder filled with a permeable medium: An analytical approach, *Heat Transf.*, 50, 2021, 3154–3175.
- [32] Anurag, Maurya, J. P., Singh, A. K., Significance of time-dependent magneto-hydrodynamic transient free convective flow in vertical annuli: An analytical approach with the finite Hankel transform, *Heat Transf.*, 50, 2021, 6719–6736.
- [33] Rajee, A., Koyani, F., Bhise, A. A., Ramesh, K., Heat transfer and entropy optimization for unsteady MHD Casson fluid flow through a porous cylinder: Applications in nuclear reactors, *Int. J. Mod. Phys. B*, 7, 2023, 2350293.
- [34] Mahian, O., Kianifar, A., Kleinstreuer, C., Al-Nimr, M. A., Pop, I., Sahin, A. Z., Wongwises, S., A review of entropy generation in nanofluid flow, *Int. J. Heat Mass Transf.*, 65, 2013, 514–532.
- [35] Mahian, O., Kianifar, A., Kalogirou, S. A., Pop, I., Wongwises, S., A review of the applications of nanofluids in solar energy, *Int. J. Heat Mass Transf.*, 57, 2013, 582–594.
- [36] Buongiorno, J., et al., A benchmark study on the thermal conductivity of nanofluids, *J. Appl. Phys.*, 106, 2009, 094312.
- [37] Choi, S. U. S., Enhancing thermal conductivity of fluids with nanoparticles, *Am. Soc. Mech. Eng. Fluids Eng. Div. FED*, 231, 1995, 99–105.
- [38] Sheikholeslami, M., Ganji, D. D., Nanofluid convective heat transfer using semi analytical and numerical approaches: A review, *J. Taiwan Inst. Chem. Eng.*, 65, 2016, 43–77.
- [39] Guo, Z., A review on heat transfer enhancement with nanofluids, *J. Enhanc. Heat Transf.*, 27, 2020, 1–70.
- [40] Mahian, O., Pop, I., Sahin, A. Z., Oztop, H. F., Wongwises, S., Irreversibility analysis of a vertical annulus using TiO<sub>2</sub>/water nanofluid with MHD flow effects, *Int. J. Heat Mass Transf.*, 64, 2013, 671–679.
- [41] Mabrouk, M., Das, D. B., Salem, Z. A., Beherei, H. H., Nanomaterials for biomedical applications: Production, characterisations, recent trends and difficulties, *Molecules*, 26, 2021, 1–27.
- [42] Wong, K. V., De Leon, O., Applications of nanofluids: Current and future, *Adv. Mech. Eng.*, 2010, 1–11.
- [43] Malik, M. Y., Naseer, M., Nadeem, S., Rehman, A., The boundary layer flow of Casson nanofluid over a vertical exponentially stretching cylinder, *Appl. Nanosci.*, 4, 2014, 869–873.
- [44] Alebraheem, J., Ramzan, M., Flow of nanofluid with Cattaneo – Christov heat flux model, *Appl. Nanosci.*, 10, 2020, 2989–99.
- [45] Khan, A., Shah, Z., Alzahrani, E., Islam, S., Entropy generation and thermal analysis for rotary motion of hydromagnetic Casson nanofluid past a rotating cylinder with Joule heating effect, *Int. Commun. Heat Mass Transf.*, 119, 2020, 104979.
- [46] Walelign, T., Haile, E., Kebede, T., Walelgn, A., Analytical study of heat and mass transfer in MHD flow of chemically reactive and thermally radiative Casson nanofluid over an inclined stretching cylinder, *J. Phys. Commun.*, 4, 2020, 1–20.
- [47] Farooq, U., Waqas, H., E.Alhazmi, S., Alhushaybari, A., Imran, M., Sadat, R., Muhammad, T., Ali, M. R., Numerical treatment of Casson nanofluid Bioconvective flow with heat transfer due to stretching cylinder/plate: Variable physical properties, *Arab. J. Chem.*, 16, 2023, 1–15.
- [48] Alharbi, K. A. M., Shahmir, N., Ramzan, M., Almusawa, M. Y., Kadry, S., Bioconvective radiative unsteady Casson nanofluid flow across two concentric stretching cylinders with variable viscosity and variable thermal conductivity, *Numer. Heat Transf. Part A-Applications*, 2023.
- [49] Mahdi, R. A., Mohammed, H. A., Munisamy, K. M., Saeid, N. H., Review of convection heat transfer and fluid flow in porous media with nanofluid, *Renew. Sustain. Energy Rev.*, 41, 2015, 715–734.
- [50] Kasaeian, A., Daneshazarian, R., Mahian, O., Kolsi, L., Chamkha, A. J., Wongwises, S., Pop, I., Nanofluid flow and heat transfer in porous media: A review of the latest developments, *Int. J. Heat Mass Transf.*, 107, 2017, 778–791.
- [51] Ghadimi, A., Saidur, R., Metselaar, H. S. C., A review of nanofluid stability properties and characterization in stationary conditions, *Int. J. Heat Mass Transf.*, 54, 2011, 4051–4068.
- [52] Merkin, J. H., Pop, I., Lok, Y. Y., Grosan, T., *Basic equations and mathematical methods, Similarity Solutions for the Boundary Layer Flow and Heat Transfer of Viscous Fluids, Nanofluids, Porous Media, and Micropolar Fluids*, Academic Press, 2022.
- [53] Yan, J. F., Liu, J., Nanocryosurgery and its mechanisms for enhancing freezing efficiency of tumor tissues, *Nanomedicine Nanotechnology, Biol. Med.*, 4, 2008, 79–87.
- [54] Yu, Z., Gao, L., Chen, K., Zhang, W., Zhang, Q., Li, Q., Hu, K., Nanoparticles: A New Approach to Upgrade Cancer Diagnosis and Treatment, *Nanoscale Res. Lett.*, 16, 2021, 88.
- [55] Hamad, E. M., Khaffaf, A., Yasin, O., El-Rub, Z. A., Al-Gharabli, S., Al-Kouz, W., Chamkha, A. J., Review of Nanofluids and Their Biomedical Applications, *J. Nanofluids*, 10, 2021, 463–477.
- [56] Hou, Y., Z. Sun, W. Rao, and J. Liu, Nanoparticle-mediated cryosurgery for tumor therapy, *Nanomedicine Nanotechnology, Biol. Med.*, 14, 2018, 493–506.
- [57] Sheikhpour, M., Arabi, M., Kasaeian, A., Rabei, A. R., Taherian, Z., Role of nanofluids in drug delivery and biomedical technology: Methods and applications, *Nanotechnol. Sci. Appl.*, 13, 2020, 47–59.
- [58] Liu, J., Deng, Z. S., Nano-cryosurgery: Advances and challenges, *J. Nanosci. Nanotechnol.*, 9, 2009, 4521–4542.
- [59] Khan, U., Bilal, S., Zaib, A., Makinde, O. D., Wakif, A., Numerical simulation of a nonlinear coupled differential system describing a convective flow of Casson gold-blood nanofluid through a stretched rotating rigid disk in the presence of Lorentz forces and nonlinear thermal radiation, *Numer. Methods Partial Differ. Equ.*, 38, 2022, 308–328.
- [60] Khan, U., Zaib, A., Khan, I., Nisar, K. S., Insight into the dynamics of transient blood conveying gold nanoparticles when entropy generation and Lorentz force are significant, *Int. Commun. Heat Mass Transf.*, 127, 2021, 105415.
- [61] Hussain, M., Farooq, U., Sheremet, M., Nonsimilar convective thermal transport analysis of EMHD stagnation Casson nanofluid flow subjected to particle shape factor and thermal radiations, *Int. Commun. Heat Mass Transf.*, 137, 2022, 106230.
- [62] Hussain, F., Nazeer, M., Altanji, M., Saleem, A., Ghafar, M. M., Thermal analysis of Casson rheological fluid with gold nanoparticles under the impact of gravitational and magnetic forces, *Case Stud. Therm. Eng.*, 28, 2021, 101433.
- [63] Upreti, H., Bartwal, P., Pandey, A. K., Makinde, O. D., Heat transfer assessment for Au-blood nanofluid flow in Darcy-Forchheimer porous medium using induced magnetic field and Cattaneo-Christov model, *Numer. Heat Transf. Part B-Fundamentals*, 84, 2023, 415–431.
- [64] Imtiaz, A., Foong, O. M., Aamina, A., Khan, N., Ali, F., Khan, I., Generalized model of blood flow in a vertical tube with suspension of gold nanomaterials: Applications in the cancer therapy, *Comput. Mater. Contin.*, 65, 2020, 171–192.



- [65] Wang, R., Chai, J., Luo, B., Liu, X., Zhang, J., Wu, M., Wei, M., Ma, Z., A review on slip boundary conditions at the nanoscale: recent development and applications, *Beilstein J. Nanotechnol.*, 12, 2021, 1237–1251.
- [66] Nubar, Y., Blood Flow, Slip, and Viscometry, *Biophys. J.*, 11, 1971, 252–264.
- [67] Khan, M., Hashim, Hafeez, A., A review on slip-flow and heat transfer performance of nanofluids from a permeable shrinking surface with thermal radiation: Dual solutions, *Chem. Eng. Sci.*, 173, 2017, 1–11.
- [68] Rao, I. J., Rajagopal, K. R., Effect of the slip boundary condition on the flow of fluids in a channel, *Acta Mech.*, 135, 1999, 113–126.
- [69] Afify, A. A., The Influence of Slip Boundary Condition on Casson Nanofluid Flow over a Stretching Sheet in the Presence of Viscous Dissipation and Chemical Reaction, *Math. Probl. Eng.*, 2017, 1–12.
- [70] Gbadeyan, J. A., Titiloye, E. O., Adeosun, A. T., Effect of variable thermal conductivity and viscosity on Casson nanofluid flow with convective heating and velocity slip, *Heliyon*, 6, 2020, e03076.
- [71] Noor, N. A. M., Shafie, S., Admon, M. A., Effects of viscous dissipation and chemical reaction on MHD squeezing flow of Casson nanofluid between parallel plates in a porous medium with slip boundary condition, *Eur. Phys. J. Plus*, 123, 2020, 855.
- [72] Thirupathi, G., Govardhan, K., Narender, G., Radiative Magnetohydrodynamics Casson Nanofluid Flow and Heat and Mass Transfer past on Nonlinear Stretching Surface, *J. Adv. Res. Numer. Heat Transf. J.*, 5, 2021, 1–21.
- [73] Usman, M., Soomro, F. A., Ul Haq, R., Wang, W., Defterli, O., Thermal and velocity slip effects on Casson nanofluid flow over an inclined permeable stretching cylinder via collocation method, *Int. J. Heat Mass Transf.*, 122, 2018, 1255–1263.
- [74] Iqbal, W., Jalil, M., Khadimallah, M. A., Hussain, M., Naeem, M. N., Al Naim, A. F., Tounsi, A., Interaction of casson nanofluid with Brownian motion: Temperature profile with shooting method, *Adv. Nano Res.*, 10, 2021, 349–357.
- [75] Azmi, W. F. W., Mohamad, A. Q., Jiann, L. Y., Shafie, S., Unsteady natural convection flow of blood Casson nanofluid (Au) in a cylinder: nano-cryosurgery applications, *Sci. Rep.*, 13, 2023, 1–15.
- [76] Rogers, K., Blood Vessel, *Encyclopedia Britannica*, 2023. Available at: <https://www.britannica.com/science/blood-vessel>.
- [77] Body, V., Blood Vessels, *Circulatory Anatomy*, 2023. Available at: <https://www.visiblebody.com/learn/circulatory/circulatory-blood>.
- [78] Tietjen, G. T., Saltzman, W. M., Nanomedicine gets personal, *Sci. Transl. Med.*, 7, 2015, 1–4.
- [79] Maiti, S., Shaw, S., Shit, G. C., Fractional order model for thermochemical flow of blood with Dufour and Soret effects under magnetic and vibration environment, *Colloids Surfaces B Biointerfaces*, 197, 2021, 111395.
- [80] Raza, J., Thermal radiation and slip effects on magnetohydrodynamic (MHD) stagnation point flow of Casson fluid over a convective stretching sheet, *Propuls. Power Res.*, 18, 2019, 138–146.
- [81] Benhanifia, K., Redouane, R., Lakhdar, B., Brahim, M., Al-Farhany, K., Jamshed, W., Eid, M. R., El Din, S. M., Raizah, Z., Investigation of mixing viscoplastic fluid with a modified anchor impeller inside a cylindrical stirred vessel using Casson–Papanastasiou model, *Sci. Rep.*, 12, 2022, 1–19.
- [82] Noranuar, W. N. N., Mohamad, A. Q., Shafie, S., Khan, I., Jiann, L. Y., Ilias, M. R., Non-coaxial rotation flow of MHD Casson nanofluid carbon nanotubes past a moving disk with porosity effect, *Ain Shams Eng. J.*, 12, 2021, 4099–4110.
- [83] Mackolil, J., Mahanthesh, B., Exact and statistical computations of radiated flow of nano and Casson fluids under heat and mass flux conditions, *J. Comput. Des. Eng.*, 6, 2019, 593–605.
- [84] Oztop, H. F., Abu-Nada, E., Numerical study of natural convection in partially heated rectangular enclosures filled with nanofluids, *Int. J. Heat Fluid Flow*, 29, 2008, 1326–1336.
- [85] Padma, R., Selvi, R. T., Ponalagusamy, R., Effects of slip and magnetic field on the pulsatile flow of a Jeffrey fluid with magnetic nanoparticles in a stenosed artery, *Eur. Phys. J. Plus*, 134, 2019, 1–15.
- [86] Khan, I., Shah, N. A., Tassaddiq, A., Mustapha, N., Kechil, S. A., Natural convection heat transfer in an oscillating vertical cylinder, *PLoS One*, 13, 2018, e0188656.
- [87] Mirza, I. A., Akram, M. S., Siddique, I., Flows of a generalized second grade fluid in a cylinder due to a velocity shock, *Chinese J. Phys.*, 60, 2019, 720–730.
- [88] Maiti, S., Shaw, S., Shit, G. C., Caputo–Fabrizio fractional order model on MHD blood flow with heat and mass transfer through a porous vessel in the presence of thermal radiation, *Phys. A Stat. Mech. its Appl.*, 540, 2020, 123149.
- [89] Esfe, M. H., Bahiraei, M., Torabi, A., Valadkhani, M., A critical review on pulsating flow in conventional fluids and nanofluids: Thermo-hydraulic characteristics, *Int. Commun. Heat Mass Transf.*, 120, 2021, 104859.
- [90] Tripathi, J., Vasu, B., Gorla, R. S. R., Chamkha, A. J., Murthy, P. V. S. N., Bég, O. A., Blood flow mediated hybrid nanoparticles in human arterial system: Recent research, development and applications, *J. Nanofluids*, 10, 2021, 1–30.
- [91] Reyaz, R., Mohamad, A. Q., Lim, Y. J., Saqib, M., Shafie, S., Analytical Solution for Impact of Caputo-Fabrizio Fractional Derivative on MHD Casson Fluid with Thermal Radiation and Chemical Reaction Effects, *Fractal Fract.*, 6, 2022, 38.
- [92] Onyiriuka, E. J., Ighodaro, O. O., Adelaja, A. O., Ewim, D. R. E., Bhattacharyya, S., A numerical investigation of the heat transfer characteristics of water-based mango bark /nanofluid flowing in a double-pipe heat exchanger, *Heliyon*, 5, 2019, e02416.

## ORCID iD

Wan Faezah Wan Azmi  <https://orcid.org/0000-0003-0430-7168>

Ahmad Qushairi Mohamad  <https://orcid.org/0000-0002-7634-5895>

Lim Yeou Jiann  <https://orcid.org/0000-0003-2506-3836>

Sharidan Shafie  <https://orcid.org/0000-0001-7795-2278>



© 2023 Shahid Chamran University of Ahvaz, Ahvaz, Iran. This article is an open access article distributed under the terms and conditions of the Creative Commons Attribution-NonCommercial 4.0 International (CC BY-NC 4.0 license) (<http://creativecommons.org/licenses/by-nc/4.0/>).

**How to cite this article:** Azmi W.F.W., Mohamad A.Q., Jiann L.Y., Shafie S. Mathematical Modelling of MHD Blood Flow with Gold Nanoparticles in Slip Small Arteries, *J. Appl. Comput. Mech.*, 10(1), 2024, 125–139.  
<https://doi.org/10.22055/jacm.2023.44057.4160>

**Publisher's Note** Shahid Chamran University of Ahvaz remains neutral with regard to jurisdictional claims in published maps and institutional affiliations.

